




# The morphology of the human mandible: A computational modelling study

Ravin Vallabh<sup>1</sup> · Ju Zhang<sup>2</sup> · Justin Fernandez<sup>2,3</sup> · George Dimitroulis<sup>4</sup> · David C. Ackland<sup>1</sup> 

Received: 31 July 2018 / Accepted: 16 February 2019 / Published online: 2 March 2019  
© Springer-Verlag GmbH Germany, part of Springer Nature 2019

## Abstract

Cephalometric methods have been used to evaluate morphometric measurements of the mandible and quantify sex-related anatomical features; however, most studies to date employ a limited set of location-specific measurements without considering the entire three-dimensional anatomy of the mandible. The aims of this study were to develop statistical shape models (SSMs) of partially edentulous male and female mandibles to evaluate inter-subject morphological variability and secondly to assess the effectiveness of discrete clinical morphometric measurements in prediction of complete three-dimensional mandible geometry. Computed tomography images of forty partially edentulous female and twenty-five male subjects were obtained, and SSM developed using mesh fitting, rigid body registration and principal component analysis. Analysis of female and male SSMs showed that the variation along their first principal components was size-related. Sex-differentiating pure shape variations were found along the first principal component of size-normalised SSM and were observed to be most prominent in the symphysis and posterior ramus regions of the mandible. Seven morphometric measurements were found to characterise female and male shape prediction optimally. The capability to rapidly generate accurate patient-specific shape-predictive models of the mandible may be useful for implant development and pre-operative planning, particularly in the absence of bony structures following trauma or tumour resection.

**Keywords** Statistical shape model · Jaw anatomy · Shape analysis · Predictive model · Morphometry · Biomechanics

## 1 Introduction

The human mandible forms the lower portion of the jaw complex and is critical in supporting teeth and facilitating mastication, speech and expression of emotion. Periodontal disease and dental caries are the most common oral

conditions leading to tooth loss—the prevalence of periodontitis in young (35–49 years) and older adults (50–64 years) is 37.2% and 52.7%, respectively (Eke et al. 2015), while 94–97% of all adults aged 35–64 years have been shown to present with dental caries (Dye et al. 2015). Following tooth loss, resorption and degradation of the alveolar bone and supporting structures may occur, as well as reduced bone ossification resulting in the formation of atrophic edentulous ridges (McGarry et al. 2002). Alveolar atrophy is a multifactorial process primarily influenced by age, sex, ethnicity, level of dentition, duration of edentulism, and biomechanical factors such as masticatory occlusal forces, which over time may affect mandibular morphology (Aragao et al. 2014; Chrcanovic et al. 2011; Huumonen et al. 2010; Nicholson and Harvati 2006; Parr et al. 2017).

The prevalence of edentulism in females is reportedly higher than that in males and has been attributed to both biological and socioeconomic factors (Peltzer et al. 2014; Russell et al. 2013). Clinical studies suggest that edentulism is associated with oestrogen deficiency, osteoporosis and periodontal disease (Brennan et al. 2007; Mohammad

---

**Electronic supplementary material** The online version of this article (<https://doi.org/10.1007/s10237-019-01133-5>) contains supplementary material, which is available to authorized users.

---

✉ David C. Ackland  
dackland@unimelb.edu.au

<sup>1</sup> Department of Biomedical Engineering, University of Melbourne, Parkville, VIC 3010, Australia

<sup>2</sup> Auckland Bioengineering Institute, University of Auckland, Auckland 1010, New Zealand

<sup>3</sup> Department of Engineering Science, University of Auckland, Auckland, New Zealand

<sup>4</sup> Department of Surgery, St Vincent's Hospital, Fitzroy, VIC 3065, Australia

et al. 2003), with geographic location also influencing its prevalence (Kailembo et al. 2017; Peltzer et al. 2014). Sex dependency of mandibular morphology may also be a key factor in dental health, since mandible shape and size are associated with load transmission between teeth and the underlying alveolar bone during mastication (Koc et al. 2010; Lin et al. 2014). At present, however, little is known about population-based variations in mandible morphology, nor the influence of sex and edentulism.

Anatomical studies have employed cephalometric methods using image datasets and cadaveric specimens to evaluate morphometric measurements of the mandible and assess sex-related anatomical differences (Aragao et al. 2014; Guler et al. 2005; Lima et al. 2016; Watanabe et al. 2010). This has included assessment of the ramus, gonion and mandibular foremen, which are anatomically significant regions for the design of temporomandibular joint replacements (Ackland et al. 2017). While there appears to be consensus in the sex-based morphological differences associated with the gonial angle, ramus and body heights (Ghosh et al. 2009; Huumonen et al. 2010; Oettle et al. 2009b), cephalometric studies may confound shape with size and employ a limited set of location-specific measurements without considering the entire three-dimensional (3D) anatomy of the mandible (Polychronis et al. 2013; Watanabe et al. 2010).

Principal component analysis (PCA) is a multivariate statistical procedure that can reduce the dimensionality of a complex three-dimensional shape across a population into a mean shape together with primary modes of variation, commonly referred to as principal components (Jolliffe 2002). Several studies have employed PCA-based statistical shape modelling to quantify sex-specific variations in dentate mandibles (Kim et al. 2012; Metzger et al. 2011; Zachow et al. 2005), with applications in development of preformed reconstructive plates (Bousleiman et al. 2013; Metzger et al. 2011; Raith et al. 2017). These methods rely on the correlation of principal component scores with clinically relevant shape predictors such as surface patches or point clouds of the bone surface, anthropological data and morphometric measurements. The capability to rapidly generate accurate patient-specific shape-predictive models of the mandible may be useful for implant development and pre-operative surgical planning, particularly when medical imaging is corrupted with metallic artefact, or the absence of bony structures following trauma or tumour resection (Zhang et al. 2016). Such techniques can also serve an important role in archaeological and forensic applications, including identification, reconstruction and finite element modelling from partial or incomplete datasets (Woods et al. 2017). At present, however, statistical shape models of the mandible have been developed only for the dentate state, and the influence of sex and dentition level on 3D mandibular geometry remains poorly understood. The aims of the present study

were therefore twofold: firstly, to develop statistically shape models of partially edentulous male and female mandibles to evaluate inter-subject morphological variability; and secondly, to assess the effectiveness of discrete clinical morphometric measurements in prediction of complete 3D mandible geometry.

## 2 Materials and methods

### 2.1 Participants

Forty female (mean age  $50.3 \pm 7.8$  years, range 39–62 years) and twenty-five male subjects (mean age  $49.5 \pm 4.9$  years, range 41–60 years) selected for temporomandibular joint replacement surgery were recruited from a local hospital. All subjects were categorised as Kennedy Class I–III and presented with 1 to 4 absent teeth excluding the third molars. Specifically, 44%, 24%, 24% and 8% of males were missing 1, 2, 3 and 4 teeth, respectively. For the females, 35%, 42.5%, 20% and 3% were missing 1, 2, 3 and 4 teeth, respectively. Subjects had no evidence of skeletal mandibular disease and no history of previous oral and maxillofacial surgery. Ethical approval for this study was obtained through the Institution's Human Ethics Advisory Group.

### 2.2 Medical imaging

Computed tomography (CT) images were obtained of each subject's entire mandible using an iCAT FLX machine (Danaher Corporation, Washington, DC, USA) with a  $120 \text{ mm} \times 140 \text{ mm}$  field of view, 14.7 s exposure time and 0.25 mm voxel size. Each subject's mandible was segmented using both manual and semi-automatic methods using 3D thresholding and interpolation (Amira FEI 5.3.3, FEI Visualization Sciences Group, Bordeaux, France). The crown and neck of teeth were excluded from the segmentation process to eliminate dentition as a modelling variable. The resulting surfaces were smoothed and decimated into 1 mm triangles (Geomagic Wrap 2014, 3D Systems, North Carolina, USA).

### 2.3 Statistical shape model generation

A combined training set of all male and female meshes ( $n = 65$ ) was used to build one size-normalised SSM to explore sex-dependent morphological features of the mandible. In addition, independent training sets of male ( $n = 25$ ) and female meshes ( $n = 40$ ) were used to develop one non-size-normalised male SSM and one size-normalised female SSM to evaluate morphological properties in male and female mandibles, respectively. The present study adopted triangulated male and female meshes which resulted in a mean root mean squared (RMS) mesh fitting error of

0.33 mm  $\pm$  0.09 mm across all three training sets (see Supplementary Material).

The generation of each SSM followed previously established methods and was comprised of (1) mesh fitting, (2) rigid body registration and (3) PCA (Zhang et al. 2014). First, mesh fitting was performed to facilitate rigid body registration of groups of mandibles and allow each mesh to be expressed in a common vector space. This was achieved by matching the orientation of all meshes in a given training set to that of one reference mandible mesh of typical size and shape using radial basis function (RBF) registration. SSM generation, PCA and data analysis were performed using MATLAB 2014 (Mathworks, USA). Open Source scripts written in Python were also employed for SSM generation, including GIAS2 and Scikit-learn.

Rigid body registration was then performed to align all registered meshes to the reference mesh using a local anatomical coordinate system, defined with the origin at the midpoint between the condyles, the  $x$  axis in the direction of the left condyle, the  $y$  axis directed posteriorly and the  $z$ -axis perpendicular to the plane formed by the  $x$  and  $y$  axes. Each fitted mesh was aligned to the reference mesh by finding the rigid translations and rotations that minimised the sum of squared distances between corresponding surface nodes.

For each of the three training sets (i.e. combined male and female meshes, male meshes and female meshes), a PCA was undertaken on the corresponding nodes of each registered mesh (Jolliffe 2002). Point coordinates of each registered mesh were concatenated into a vector,  $\mathbf{x} = [x_1, y_1, z_1, x_2, y_2, z_2, \dots, x_n, y_n, z_n]$ , where  $x_n, y_n, z_n$  are the 3D coordinates of  $n$  nodes. The coordinate vectors

were then assembled into a data matrix of the form  $\mathbf{X} = [\mathbf{x}_1, \mathbf{x}_2, \dots, \mathbf{x}_m]^T$ . PCA was performed on  $\mathbf{X}$  using singular value decomposition (SVD), which allowed any shape variation  $\mathbf{x}$  in the training set to be approximated as the mean  $\bar{\mathbf{x}}$  plus the weighted sum of the first  $k$  principal components,  $\mathbf{b}$

$$\mathbf{x} = \bar{\mathbf{x}} + \sum_{i=1}^k a_i \mathbf{b}_i \quad (1)$$

The PCA yielded a SSM for which the principal components of morphological variation within the training set were evaluated and used in subsequent analyses. A mean mandible geometry was calculated for each of the non-size-normalised male and female SSMs.

## 2.4 Morphometric measurements

Twelve anatomical landmarks (Table 1) and twelve morphometric measurements of clinical relevance adapted from previous studies (Bayome et al. 2013; Bräuer 1988; Chrcanovic et al. 2011) (Table 2) were manually identified on each male and female surface mesh of all 65 mandibles (Fig. 1). These landmarks and morphometric measurements were also identified on the mean non-size-normalized male and female SSMs. Morphological measurements were evaluated on four randomly selected female meshes at 3-day intervals, and the intraclass correlation coefficient (ICC) was used to calculate intra-observer reliability and reproducibility.

**Table 1** Descriptions of landmarks used to derive mandibular morphometric measurements (see Table 2), adapted from previous studies (Bayome et al. 2013; Chrcanovic et al. 2011)

Anatomical landmark		Description
Anterior border	AB	Border that separates the coronoid process and the oblique line
Anterior inferior border	$B_{\text{ant,Inf}}$	The most anterior and inferior prominence of the mandible
Anterior infradentale	$I_{\text{Ant}}$	The most prominent anterior midline point of the mandible alveolar process
Anterior lateral alveolar process	$AP_{\text{Ant,Lat}}$	The most prominent anterolateral point the thickened ridge of mandibular bone that contains the dental alveoli
Inferior lateral gonion	$GO_{\text{Inf,Lat}}$	The most prominent posterior, inferior point along the rounded corner of the mandible between the mandibular ramus and the mandibular body
Lateral condyilion	$CO_{\text{Lat}}$	The most prominent lateral point on the mandibular condyle
Mandibular notch	MN	The deep concavity that separates the coronoid process anteriorly and the condyloid process posteriorly
Medial condyilion	$CO_{\text{Med}}$	The most prominent medial point on the mandibular condyle
Pogonion	Po	The point on the bony symphysis tangent to the facial plane
Posterior condyilion	$CO_{\text{Pos}}$	The most prominent posterior point on the mandibular condyle
Posterior mandibular ramus	$MR_{\text{Pos}}$	The most prominent posterior point on the mandibular ramus

Mandibular landmarks include the anterior border, anterior inferior border, anterior infradentale, anterior lateral alveolar process, inferior lateral gonion, lateral condyilion, mandibular notch, medial condyilion, pogonion, posterior condyilion and posterior mandibular ramus

**Table 2** Descriptions of mandibular morphometric measurements used in mandibular shape prediction, adapted from previous studies (Bayome et al. 2013; Bräuer 1988; Chrcanovic et al. 2011)

Morphometric Measurement		Description
Body height	$B_H$	The distance from the anterior lateral alveolar process to the inferior border of the mandible, perpendicular to the base at the level of the mental foramen
Body length	$B_L$	The distance of the anterior margin of the mental region from a centre point on the line between the posterior border of the two mandibular angles
Body width	$B_W$	The maximum width of the mandibular body, measured in the region of the mental foramen perpendicular to the long axis of the mandibular pole
Condyle height	$C_H$	The perpendicular distance between the superior condyilion and the axis of the lowest point of the mandibular notch perpendicular to plane intersecting the posterior condyilion and the posterior mandibular ramus
Gonial angle	$G_A$	The angle between a line tangent to the lower border of the mandible and a line tangent to the posterior border of the mandibular ramus
Intercondylar angle	$Ic_A$	The angle formed between two lines coincident with the long axis of each condylar pole
Intercondylar distance	$Ic_D$	The distance between the most lateral prominences on the left and right lateral condyles
Intergonial distance	$Ig_D$	The distance between the most prominent inferolateral points on the left and right gonion
Pogonion–interdental distance	$PoIn_D$	The perpendicular distance between the anterior infradentale and the pogonion
Pogonion–lateral condylar distance	$PoLaCo_D$	The distance between the pogonion and the lateral condyle
Ramus height	$R_H$	The distance between the superior condyilion and the lateral gonion
Ramus width	$R_W$	The shortest breadth of the mandibular ramus measured perpendicular to the line tangent to the posterior border of the mandibular ramus

Morphometric measurements include mandibular body height, body length, body width, condyle height, gonial angle, intercondylar angle, intercondylar distance, intergonial distance, pogonion–interdental distance, pogonion–lateral condylar distance, ramus height and ramus width

## 2.5 Mandible shape prediction

Each of the male mandible meshes was individually predicted using the SSM derived from the complete training set of male mandibles less the given mandible mesh. The predicted mandible geometry was then directly compared with the known mandible geometry derived from the segmented image dataset. This mandible prediction process was repeated for all female mandible geometries.

The male and female mandible geometries were predicted using a univariate least absolute shrinkage and selection operator (Lasso) regression model that calculated the first principal component scores of the mandible from its training set. The mandible meshes were then reconstructed from the scores using Eq. (1) (Tibshirani 1996). Bayesian information criteria (BIC) were used to control the Lasso regression model's regularisation to select the optimal (smallest) number of morphometric measurements to produce the highest mandibular geometry prediction accuracy. This criterion made a trade-off between the goodness of fit and the complexity of the model. An ensemble of Lasso regressors,  $\mathbf{R} = \{R_{1\dots k}\}$ , were used to predict the first  $k$  principal component scores,  $\hat{a}_{i\dots k}$ , and thus the mandible shape using

$$\hat{a}_i = R_i(\mathbf{m}_i) \quad (2)$$

where  $\mathbf{m}_i \in \mathbf{m}$ , i.e.  $\mathbf{m}_i$  is a subset of all given measurements  $\mathbf{m}$ .

The number of principal component scores was selected by training ensembles  $\mathbf{R}_{k=1}$  to  $\mathbf{R}_{k=10}$  and picking the ensemble with the smallest leave-one-out RMS error between the actual and predicted surface meshes:

1. In the initial (0th) iteration,  $\mathbf{R}^0$  was found using  $\mathbf{m}^0$  containing all 12 measurements.
2. In the  $i$ th iteration, any measurements in  $\mathbf{m}^{i-1}$  not used by the regressors in  $\mathbf{R}^{i-1}$ , or the measurement used by the least number of regressors in  $\mathbf{R}^{i-1}$  were dropped out for  $\mathbf{m}^i$ . If there was a tie for the least used measurement, the measurement used to regress the scores of the higher principal components (and therefore less significant shape variations) was dropped.
3.  $\mathbf{R}^i$  was then found using  $\mathbf{m}^i$ . Note that each  $\mathbf{R}^i$  has a potentially different  $k$ ,  $k^i$ .
4. Steps 2 and 3 were repeated until only 1 measurement was left.
5. For each  $\mathbf{R}^i$ , the sum of the BICs of its ensemble regressors  $B^i(\mathbf{R}^i, \mathbf{m}^i) = \sum_{j=1}^{k^i} \text{BIC}(R_j, \mathbf{m}_j)$  was recorded. The ensemble and its corresponding measurement set with the lowest  $B$  were selected as the final optimal model:  $\mathbf{R}^*, \mathbf{m}^* = \text{argmin}_i \{B^i(\mathbf{R}^i, \mathbf{m}^i)\}$ .

The final predictive shape was constructed by projecting the principal component scores of  $k$  models within the vector space of the SSM. The capability of the SSM to

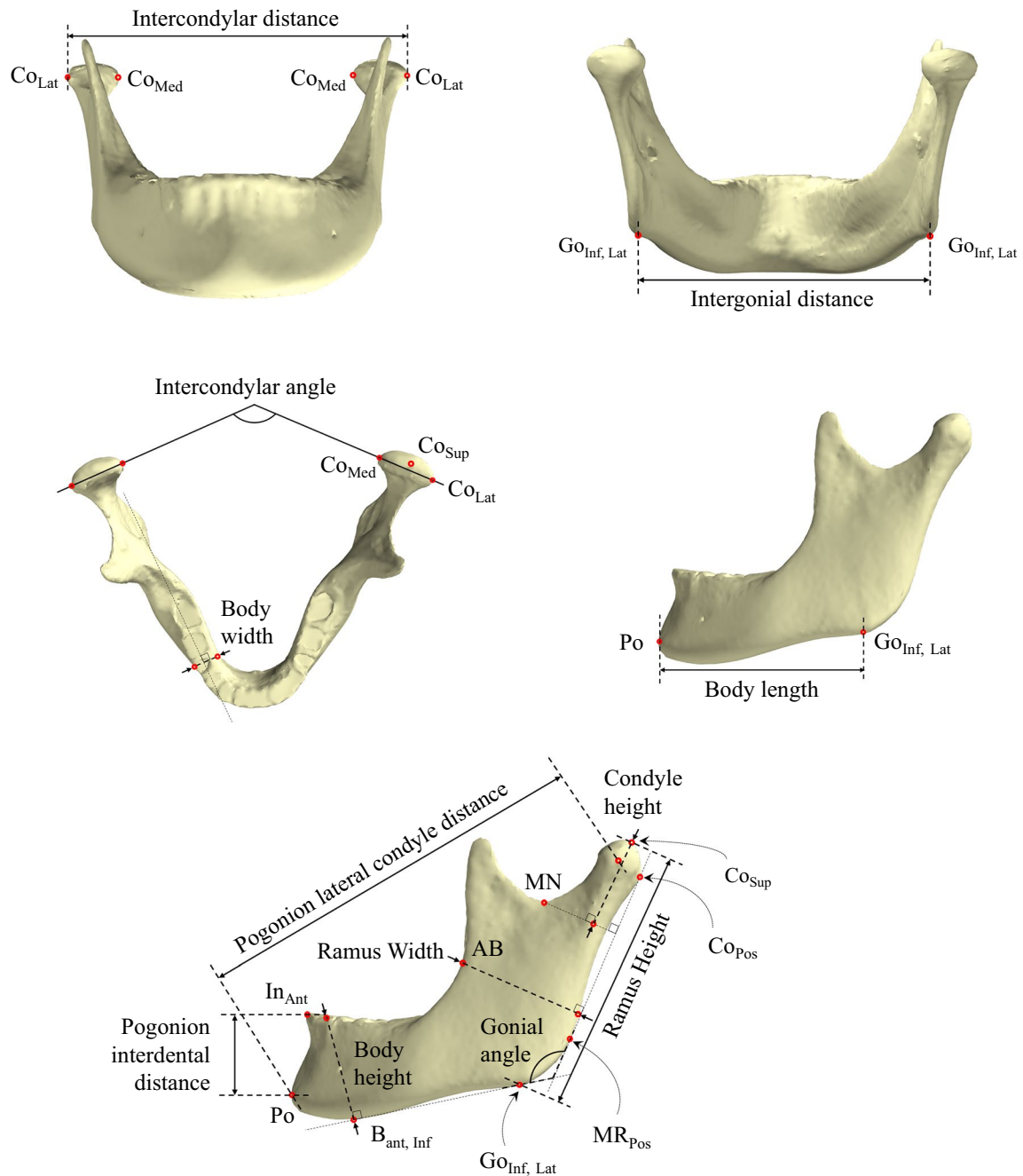


**Fig. 1** Anatomical landmarks and morphometric measurements used in mandibular shape prediction. For symbol definitions and descriptions of morphological measurements, see Tables 1 and 2

accurately approximate unseen mandibles was quantified using closest-neighbour whole surface-to-surface RMS error (Zhang et al. 2014). The RMS error was calculated between every point on the predicted mesh and the closest points on the actual mesh.

### 2.6 Data analysis

The mean and standard deviation of each morphological measurement were calculated for both male and female mandibles. Measurements were taken bilaterally, and if no

significant differences were observed between left and right sides, an average measurement from both sides was taken. Statistically significant differences in means between sexes were evaluated for each independent variable using Student's *t*-tests. The bilateral differences within a given sex were also estimated for conditioned variability. The first four significant principal component scores associated with the size-normalised shape model were extracted and classified by sex to explore sex-related shape differences along each principal component. Student's *t*-tests were used to quantify differences in shape between the first four significant principal components of female and male mandibles. Q–Q plots and Shapiro–Wilk tests were undertaken to determine normality of data, and a two-sample *F* test to confirm equal variances. An adjusted significance level was established using a Bonferroni correction to  $\alpha = 0.05/12 = 0.004$ .

### 3 Results

#### 3.1 Morphometric measurements

Large variability of the morphometric mandibular measurements was observed between female and male training sets within each sex. In females, the greatest variability was found in the condyle height, body width and pogonion–interdental distance, each having a CV of 16%. In contrast, the greatest variability in males was found in the condyle height with a CV of 19% followed by the body width which had 15% CV. Statistically significant differences between males and females were found in body height (mean difference 2.7 mm,  $p < 0.001$ ), ramus height (mean difference 1.5 mm;  $p < 0.001$ ), intercondylar distance (mean difference 6.5 mm;

$p = 0.004$ ), body length (mean difference 7.3 mm;  $p < 0.001$ ) and intergonial distance (mean difference 7.5 mm;  $p < 0.001$ ) (Table 3). The ICC between the repeated measurements showed good reliability, with a range 0.79 to 0.96.

#### 3.2 Non-size-normalised mandible morphology

PCA on the female and male mandible training sets produced non-size-normalised SSMs in which 95% of the sample variation was explained in the first twenty and fifteen principal components, respectively (Fig. 2). The first four significant principal components of each SSM captured 61.1% and 74.6% of the variation present in the male and female training sets, respectively. The variation along the first principal components of the female and male mandible SSMs was dominated by size.

In females, the body and ramus widths, pogonion–interdental distance and condylar head shape influenced the variation along second principal component (Table 4). Two standard deviations from the mean along the second principal component in the female SSM showed the superior surface of the condylar head becoming more convex (Fig. 3). The predominant variations exhibited along the third principal component were the gonial angle and ramus height, with the morphological changes observed along this principal component being relatively small. The body height at the third molar region became substantially thinner as the third principal component scores increased in the positive direction. The pogonion–lateral condylar distance was shown to be the prominent variation along the fourth principal component. When varied between plus and minus two standard deviations, a 64% difference in measured value was observed. As the fourth principal component scores became

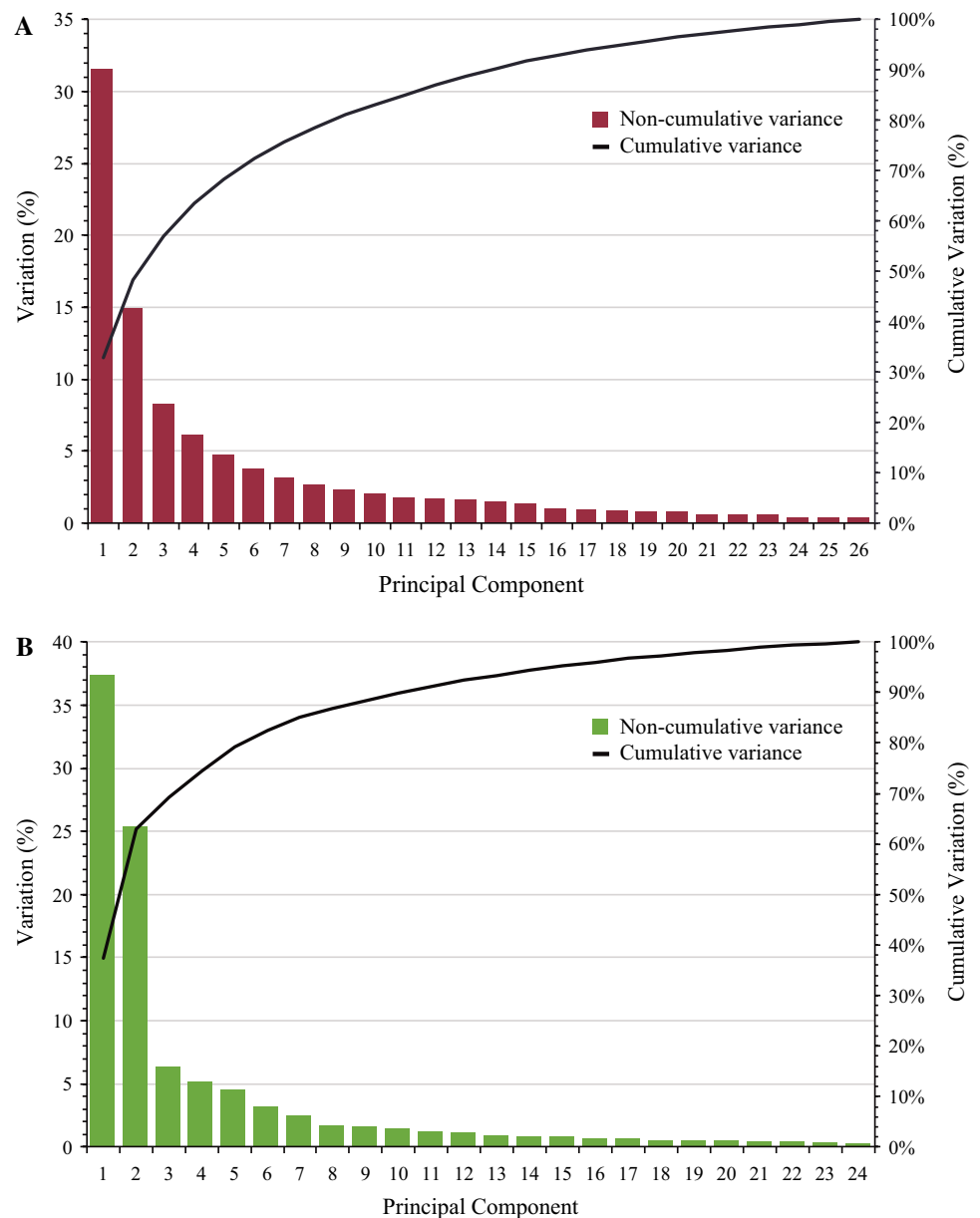
**Table 3** Summary of morphometric measurements taken from mandibular surface meshes using male and female training sets as well as from each mean non-size-normalised statistical shape model (SSM)

	Female		Male	
	Training set	Mean SSM	Training set	Mean SSM
Condyle height	18.8 (3)	19.5	19.9 (3.8)	20.2
Pogonion–lateral condylar distance	114.3 (4.5)	114.7	120.0 (4.8)	119.9
Body height	27.0 (2.5)	26.7	29.7 (2.8)	29.8*
Body width	11.4 (1.8)	10.2	11.9 (1.8)	12.0
Ramus height	61.5 (5.0)	61.0	70.4 (6.2)	69.6*
Ramus width	29.2 (2.5)	29.8	31.1 (3.2)	31.7
Gonial angle	126.1 (6.1)	128.2	121.0 (8.1)	121.3
Intercondylar angle	133.8 (16.8)	128.2	134.7 (14.4)	134.7
Pogonion–interdental distance	21.9 (3.5)	22.2	22.3 (4.2)	21.4
Intercondylar distance	115.2 (6.6)	114.8	121.7 (7.0)	120.8*
Body length	72.4 (5.1)	72.7	79.7 (5.6)	78.6*
Intergonial distance	86.0 (4.9)	86.2	93.5 (5.7)	92.9*

Mean data and standard deviation (in parentheses) are given

\*Statistically significant difference in a morphological measurement between males and females. Significance level was set at  $p \leq 0.004$ . Angles are given in degrees and length measurements in millimetres

**Fig. 2** Percentage geometric variation and cumulative variation captured by the principal components of the female (a) and male (b) mandibles



more positive, the condylar head became smaller and more rounded.

For males, the condylar height was one of three prominent variations observed along the second and third principal components with percentage changes of 46% and 43% between plus and minus two standard deviations along these principal components, respectively. The superior surface of the condylar head shape flattened as the first, third and fourth principal component scores became more positive (Fig. 4). As the second principal component scores increased from minus two standard deviations to plus two standard deviations, the body and ramus widths exhibited a 58% and 36% increase, respectively. Variation in gonion eversion

was captured along the second, third and fourth principal components.

### 3.3 Sex-dependent shape variations

PCA on the combined training set of male and female meshes produced a size-normalised SSM in which 95% of the variation was captured in the first sixteen principal components (see Supplementary Material). The first four significant principal components captured 70.6% of the variation present in the combined training set with the first principal component alone captured 46.6% of the variation. Subsequent principal components were not

**Table 4** Mandibular morphometric measurements that are most strongly associated with the first four principal components of the non-size-normalised male and female statistical shape model

Principal component	Female		Male	
	Morphometric measurement	Range	Morphometric measurement	Range
1	Body width	11.3–9.1	Condyle height	21.1–17.3
	Ramus height	65.6–56.7	Body width	10.9–12.6
	Intercondylar distance	126.0–103.6	Ramus width	29.5–33.9
	Intergonial distance	92.5–81.8	Intercondylar distance	110.5–132.2
2	Condyle height	17.7–20.1	Condyle height	15.6–22.8
	Pogonion–lateral condylar distance	108.8–119.8	Pogonion–lateral condylar distance	110.6–133.0
	Body height	23.7–28.9	Body height	25.5–33.3
	Body width	9.3–11.7	Body width	8.9–14.2
	Body length	65.5–80.7	Body length	72.5–85.6
	Ramus height	56.1–65.7	Ramus width	27.2–36.9
	Ramus width	26.0–32.8	Intercondylar angle	129.5–148.5
	Intercondylar angle	119.2–143.8	Pogonion–interdental distance	20.9–25.6
	Pogonion–interdental distance	19.6–24.6	Intergonial distance	87.1–98.5
	3	Ramus height	64.3–57.1	Condyle height
Gonial angle		122.3–137.1	Body height	28.0–31.3
			Body width	10.7–13.1
			Pogonion–interdental distance	20.9–25.8
4	Pogonion–lateral condylar distance	69.3–112.8	Intercondylar distance	96.8–86.6
	Body height	28.9–23.7	Condyle height	19.2–16.9
	Pogonion–interdental distance	24.4–16.0	Ramus width	34.5–30.3
			Intercondylar angle	146.9–130.5
		Intergonial distance	98.4–80.3	

Shown are the morphometric measurements that changed more than 10% of their initial value when perturbed between  $-2.0$  standard deviations and  $+2.0$  standard deviations along each principal component. Angles are given in degrees and length measurements in millimetres

considered significant due to the small change in the gradient of the cumulative variation curve (Fig. 2).

Statistically significant differences were found in the first principal component scores of the size-normalised shape model between males and females ( $p < 0.001$ ), indicating that this principal component represents a significant mode of sex-differentiating pure shape variation (Fig. 5). The sex-specific morphological differences observed were most prominent in the symphysis region. Males typically displayed a wider and vertically higher mental symphysis, rather than a rounded mental symphysis as observed in females. The mental eminence (point of chin) was squarer and less projected in males. In the posterior corpus region, males exhibited a wider and greater ramus height, gonial angles were closer to  $90^\circ$ , and eversion was more pronounced while the ascending ramus was broader. There were no sex-specific significant differences along any other principal components ( $p > 0.004$ ).

### 3.4 Shape prediction

Seven morphometric measurements were shown to produce the smallest BIC and were thus selected as the optimal female mandible geometry predictors for the stepwise Lasso regression model (Fig. 6a), and similarly, seven morphometric measurements produced the smallest BIC and were selected as the optimal male mandible geometry predictors (Fig. 6b). Six of these morphometric measurements were common to male and female mandibles: pogonion–lateral condylar distance, ramus height, intercondylar distance, ramus width, pogonion–interdental distance and body length. The additional of condylar height and intergonial distance was required to predict male and female mandible shapes, respectively.

The first seven significant principal components derived from the female non-size-normalised shape model (using the seven optimal morphometric measurements) were required to perform accurate female shape predictions and produce



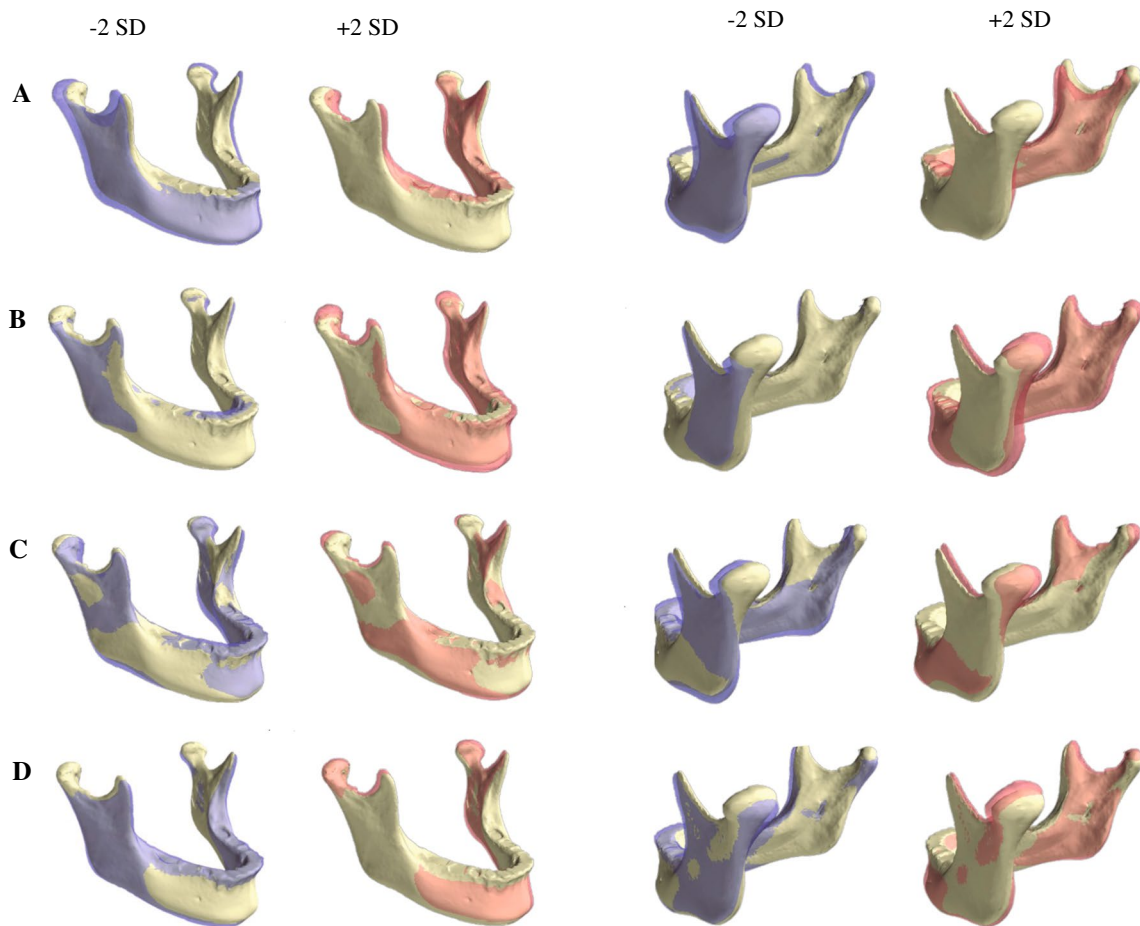


**Fig. 3** Illustration of the first four principal components of the female non-size-normalised SSM. Mandibular shapes are given for  $-2$  standard deviations (transparent blue) and  $+2$  standard deviations (transparent red) superimposed on the mean mandible shape along

the first principal component (**a**), second principal component (**b**), third principal component (**c**) and fourth principal component (**d**). Anterior isometric views are given on the left, and posterior isometric views on the right

a leave-one-out RMS error of 1.29 mm, which was within 0.03 mm of the female mandible model derived from all twelve morphometric measurements. The first three principal components derived from the male non-size-normalised shape model (using the seven optimal morphometric measurements) were necessary for accurate male shape prediction, producing a leave-one-out RMS error of 1.47 mm, which was 0.02 mm less than the male mandible model derived from all twelve morphometric measurements.

Female shape prediction error was greatest on the ramus, gonion and condylar process, while the body and symphysis were better predicted (Fig. 7a). The overall male shape prediction error was prevalent on a greater area of the mandible, whilst isolated regions on the body were better predicted (Fig. 7b). Consistent with the closest-neighbour surface error maps, statistically significant differences were found in the ramus height between the male actual and predicted meshes (Fig. 8). The smallest mean morphometric measurement differences between the actual and predicted models

were observed in the condylar height, body width and ramus width.

## 4 Discussion

The purpose of this study was to develop a PCA-based statistical shape modelling framework to characterise the inter-subject morphological variability of partially edentulous human mandibles selected for TMJ replacement surgery. While SSMs have been previously used to predict anatomical variability of bony structures (Bah et al. 2015), we assessed the capability of SSMs to predict complete 3D mandibular surface geometry using a selection of discrete clinical morphometric measurements. Analysis of female and male SSMs showed that the variation along their first principal components was size-related. Sex-differentiating pure shape variations were found along the first principal component of the size-normalised shape model and were observed to

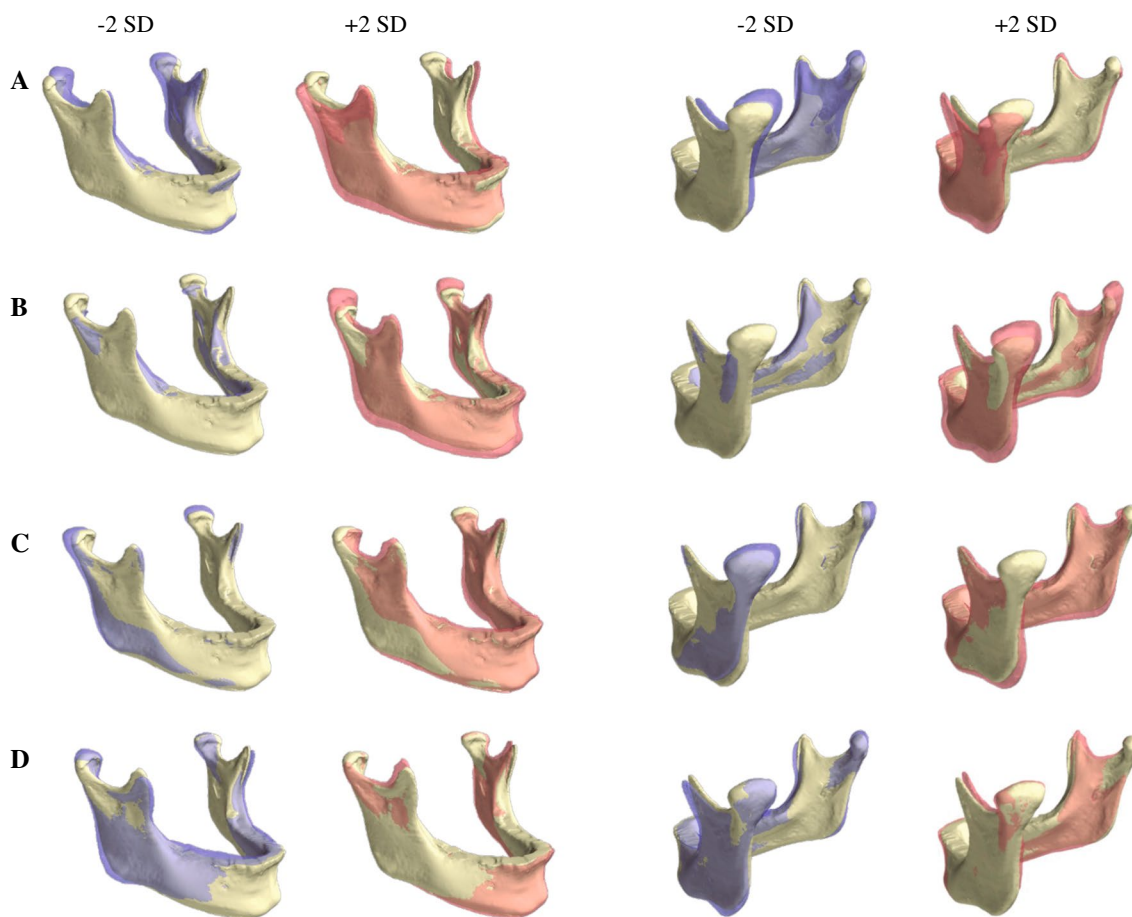


**Fig. 4** Illustration of the first four principal components of the male non-size-normalised SSM. Mandibular shapes are given for  $-2$  standard deviations (transparent blue) and  $+2$  standard deviations (transparent red) superimposed on the mean mandible shape along

the first principal component (a), second principal component (b), third principal component (c) and fourth principal component (d). Anterior isometric views are given on the left, and posterior isometric views on the right

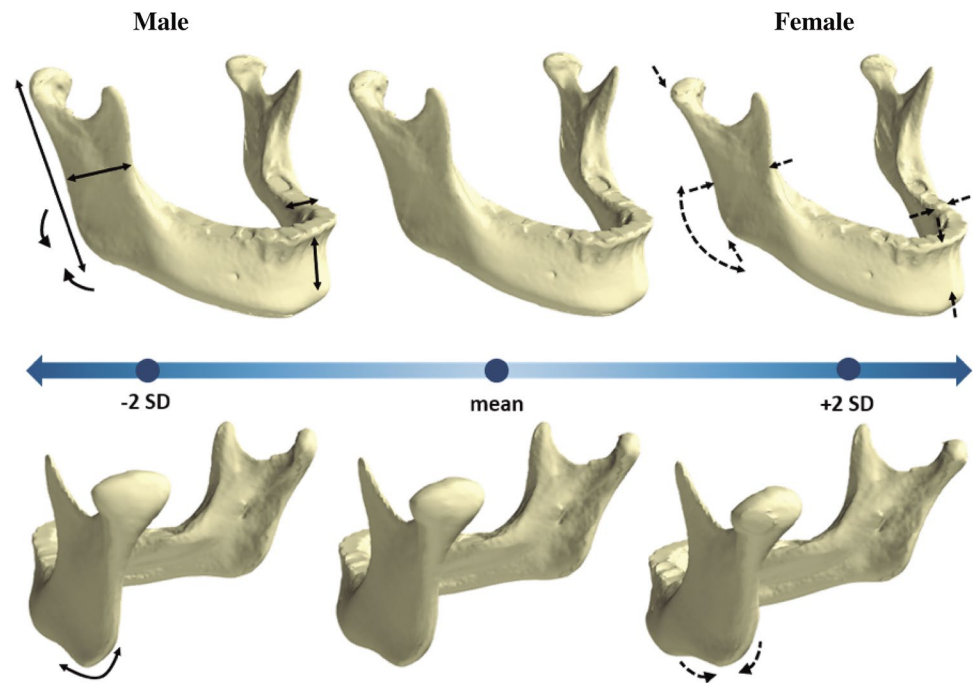
be most prominent in the symphysis and posterior ramus regions of the mandible. Seven morphometric measurements were found to characterise female and male shape prediction optimally, resulting in leave-one-out RMS errors less than 1.47 mm.

Our strategy of building SSMs, which included mesh fitting, rigid body registration and PCA, has been used previously to characterise morphological geometry and material properties of teeth in archaeological research (Woods et al. 2017), as well as quantify anatomy of the carpometacarpal joint (Schneider et al. 2015); however, we adopted a RBF-based non-rigid registration to morph a reference mesh to the training set shapes, which avoided manually building a reference mesh, and resulted in lower RMS errors (0.33 mm, compared to 0.41 mm in Schneider et al. 2015). The advantages of RBF registration are that no pre-selection of landmarks is required to constrain the fitting process, and the RBF algorithm determines the closest corresponding nodes between the template mesh and the target. In addition, the

algorithm iteratively adds RBF nodes to the target mesh to improve registration error in regions of high error. The selected reference template mandible meshes had no visible geometric artefacts such as mesh torsion on the surfaces of the SSMs, suggesting that artificial variations and geometric artefacts were not introduced during the SSM creation process. RMS errors between 0.5 and 0.7 mm, with no visible geometric artefacts, have been reported when implemented on training sets of the femur and pelvis (Zhang et al. 2018).

Measurements of body length, body height, ramus height, gonial angle and intergonial distance on the mean female and male non-size-normalised SSMs were similar to those recorded by Ozturk et al. 2013 and Parr et al. 2017 on partially edentulous cadaveric specimens of age 41–64 years (Table 5) (Ozturk et al. 2013; Parr et al. 2017). For example, the female body length found in the present study was 72.9 mm, while Ozturk et al. 2013 and Parr et al. 2017 obtained 72.8 mm and 73.6 mm, respectively. In contrast, the pogonion–interdental distance in the present study

**Fig. 5** Mandibular shape differences demonstrated along the first principal component of the size-normalised SSM. Shown is the mean SSM from the combined male and female training set (centre),  $-2$  standard deviations along the first principal component using the male dataset (left) and  $+2$  standard deviations along the first principal component using the female dataset (left)



(for example, 21.7 mm in males) was notably different to that measured by Ozturk et al. 2013 and Parr et al. 2017 (27.3 mm and 32.9 mm, respectively). This discrepancy may be due to different sample compositions and the alternative cephalometric methods employed and suggests that larger sample sizes are required to improve the ability of the mean SSMs to accurately represent mean bone geometries in a population (Raith et al. 2016).

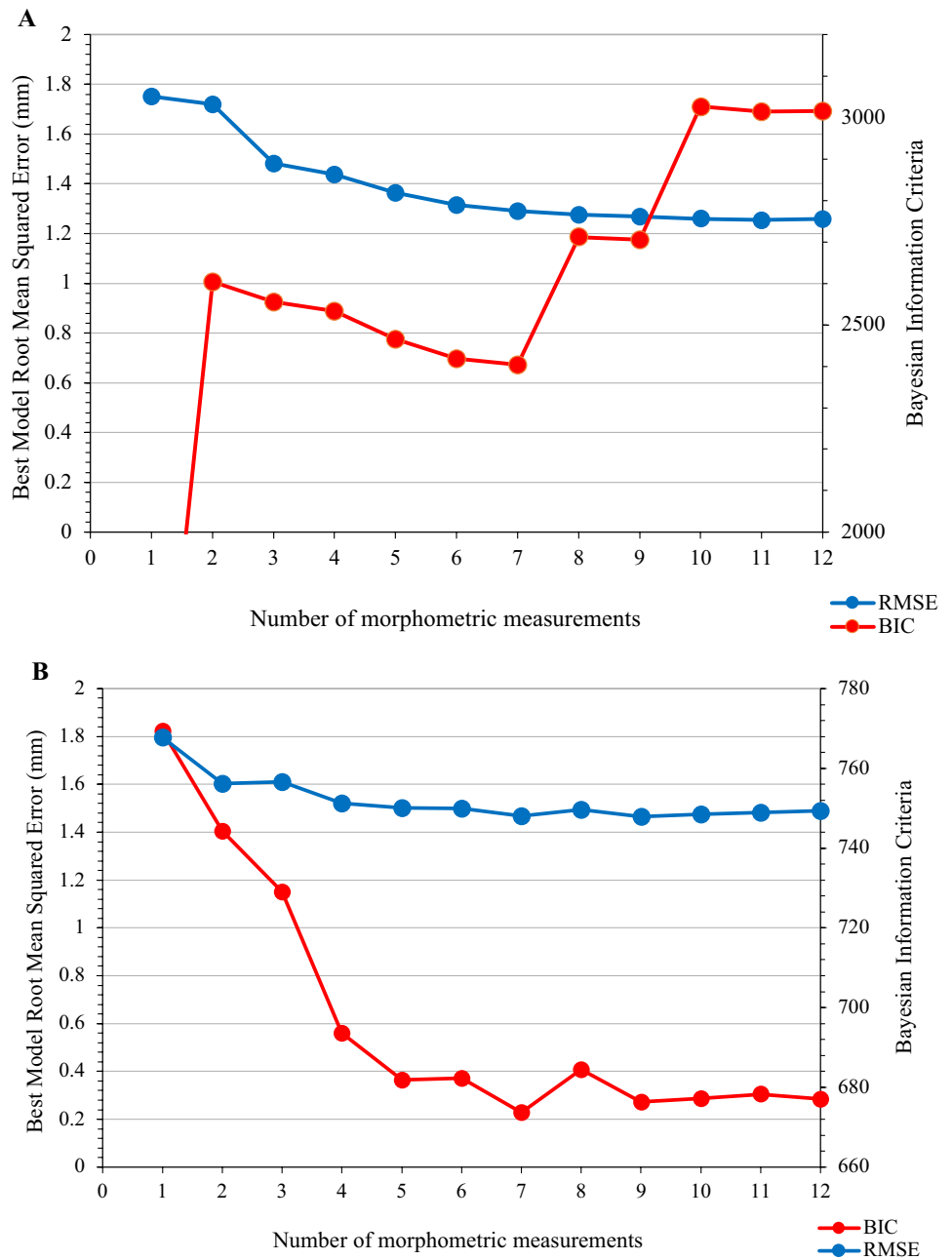
Analysis of the female and male non-size-normalised SSMs of partially edentulous mandibles showed that the dominant variation along the first principal components was size-related, indicating the presence of allometry. This finding is in agreement with that from previous population studies utilising PCA-based SSM approaches, including those investigating morphology of the femur, knee and carpometacarpal joint bones (Bah et al. 2015; Chan et al. 2013; Schneider et al. 2015; Smoger et al. 2017). Males displayed a narrower gonial angle of between  $90^\circ$  and  $120^\circ$ , while females exhibited a neutral gonial angle between  $120^\circ$  and  $130^\circ$ , which has been demonstrated in previous cephalometric studies (Bousleiman et al. 2013; Cocos and Halazoneitis 2017; Franklin et al. 2007). Gonion eversion was also observed to be distinct in males, as has long been identified as a dimorphic trait for male sex determination (Chrcanovic et al. 2011; Oettle et al. 2009a). Also compared to previous studies, males exhibited ramus flexure at the level of the occlusal plane of the molars and was observed near the condylar neck in females (Balci et al. 2005; Hwang et al. 2015; Lin et al. 2014; Loth and Henneberg 1996). Although considered a male dimorphic trait, ramus flexure was apparent in both sexes along the second principal component

(Kemkes-Grottenthaler et al. 2002). These findings have possible implications in between-sex forensic identification of mandible samples.

It has been suggested that morphological variations in the mandible between and within sexes reflect masticatory muscle function (Koc et al. 2010; Lin et al. 2013). For example, male and female mandibles with larger masticatory muscle cross-sectional areas have been associated with a wider and more trapezoidal ramus, a larger coronoid and a more curved basal arch (Sella-Tunis et al. 2018). Bone size has implications on the masticatory muscle forces and therefore bite force, as well as the stresses incurred by the mandible, since geometric size variations influence the area of the insertion of the musculature as well as the moment arms of the masticatory muscles about the TMJ. Specifically, posterior mandibular shape, the mandibular inclination and the extent of gonial angulation may influence muscle architecture between-sex. The findings of the present study show a more vertical ramus and acute gonial angle in partially edentulous males may lead to greater mechanical advantage during mastication than that in females. These findings may be associated with sex-specific bite force generation and mandibular bone mineral density distribution, which ought to be explored in future studies as determinates of mandible function.

The Lasso regression model with L1 regularisation predicted the full 3D morphology of unseen female and male mandibles to within a leave-one-out RMS error of 1.8 mm using all twelve digitised morphometric measurements as shape predictors. Progressive improvement in the female prediction error was observed, the more morphometric

**Fig. 6** RMS error and number of measurements derived from the Bayesian information criterion-based Lasso model used to determine the optimal set of morphometric measurements to best describe mandible geometry with the female (a) and male training sets (b)

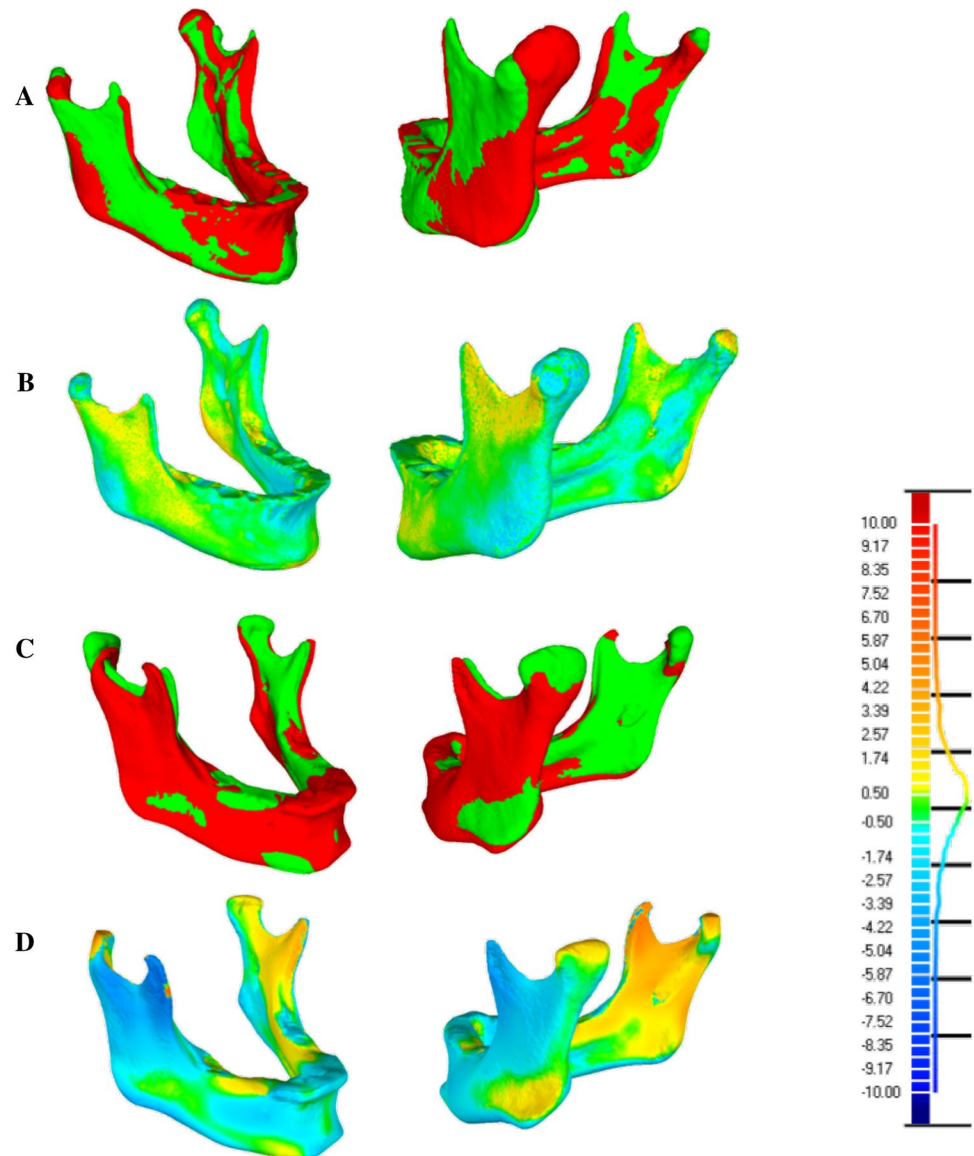


measurements were employed to constrain the regression model. However, for males, inclusion of more than seven key morphometric measurements did not improve shape prediction accuracy. The relatively high coefficient of variations of the last five measurements selected to constrain the model (ramus width, intercondylar distance, condylar height, body height and body length) may have attributed to the lack of prediction improvement in the male mandible.

The SSM, constrained by seven optimal measurements, predicted female and male shapes to within leave-one-out RMS errors less than 1.5 mm. Female prediction errors were found at the ramus, gonion and condylar head, resulting from

the gonial angle and condylar height measurements being left unconstrained. Male shape prediction errors were found on the ramus and gonion, which were likely due to the intergonial distance being left unconstrained. Although condylar height was constrained, the large coefficient of variation of this measurement may have contributed to the prediction errors observed on the condylar head. Gonion eversion is a non-metric parameter which is thought to further contribute to the prediction errors in the gonion region for both sexes. Despite these errors, the BIC was shown to be effective in selecting the optimal subset of morphometric measurements to predict mandibular geometry. This technique may

**Fig. 7** Shape prediction data for a representative female and male mandible. Shown are a female subject's actual (red) and predicted (green) mandible shape (a), and the corresponding closest-neighbour whole surface-to-surface RMS error in mm (b), as well as a male subject's actual (red) and predicted (green) mandible shape (c), and the corresponding closest-neighbour whole surface-to-surface RMS error in mm (d)



be useful as a tool for predicting patient-specific mandible anatomy in reconstructive surgery, for example, when bony geometry of one side of the mandible is not available due to pathology or trauma. While the present study employed CT images for surface geometry reconstruction and SSM development, future studies ought to adapt the methods presented to lower-dose imaging modalities used clinically, including orthopantomogram (OPG).

The results showed that the BIC continued to increase when using more than 7 morphometric measurements to describe the mandibular geometry with the female mandible dataset, while the BIC tended to plateau at 7 morphometric measurements when using the male mandible dataset. We developed a combined-sex SSM using all 65 mandibles and then used it to train two predictive SSMs: one using the union set of the optimal male and female measurements

(8 measurements) and another using the intersection set (6 measurements). The union set model achieved a leave-one-out RMS error of 1.38 mm, while the intersection set model achieved a leave-one-out RMS error of 1.46 mm. While this model error improves with the male-only model, it is worse than that in the female-only model, suggesting that sex-specific models are better for shape prediction. However, the difference in training set composition and size for the male, female and combined models creates confounding effects. The female training set is nearly double that of the male set and could be a reason for the error difference between the male and female SSMs. A larger male training set may improve the error of the male SSM and the combined male and female SSM.

There are some limitations that ought to be considered before interpreting the findings of this study. Firstly,

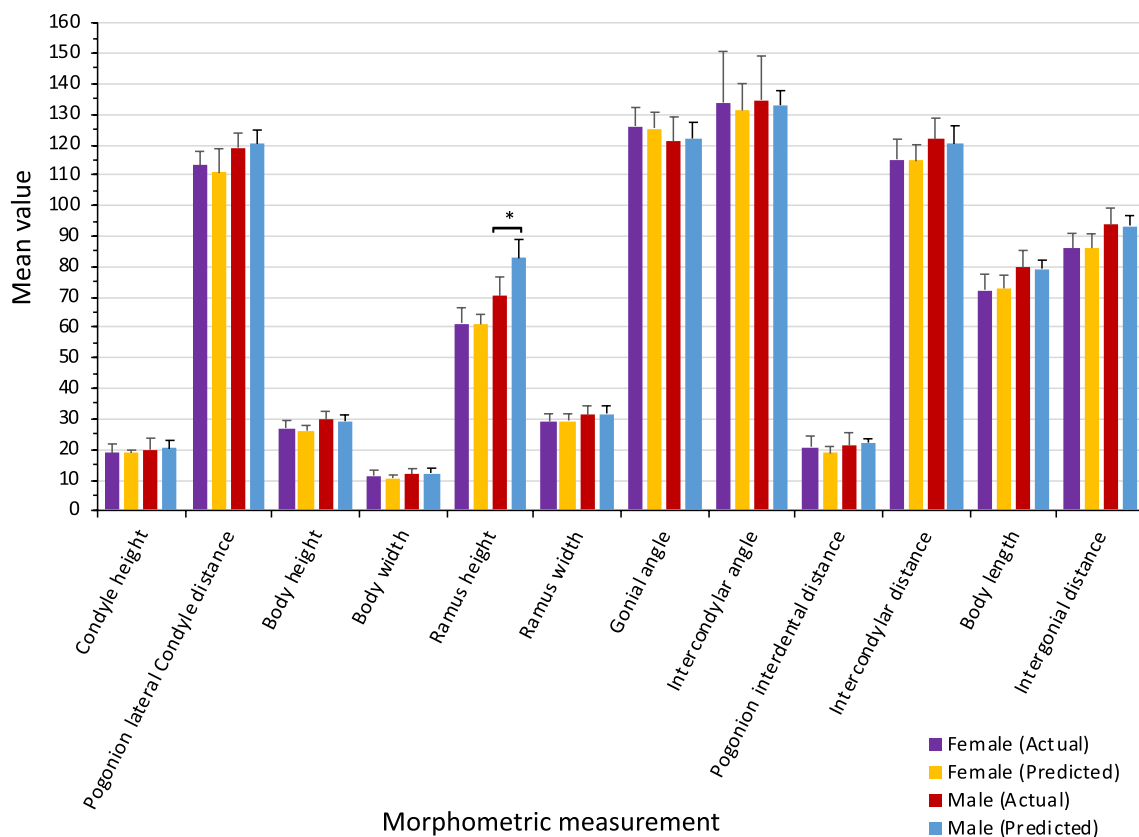


**Fig. 8** Comparison of mean values of morphometric measurements between actual and predicted female and male SSMs. An asterisk denotes a statistically significant difference between the actual and

predicted shape model for  $p < 0.004$ . Angles are given in degrees and length measurements in millimetres

**Table 5** Comparison of morphometric measurements determined in the present study using non-size-normalised statistical shape models (SSM) with those in cephalometric studies by Ozturk et al. (2013) and Parr et al. (2017)

	SSM		Ozturk et al. (2013)		Parr et al. (2017)	
	Female	Male	Female (range)	Male (range)	Female (standard deviation)	Male (standard deviation)
Body length	72.9	78.6	72.8 (69.6–76.1)	75.1 (71.5–78.6)	73.6 (5.8)	78.3 (5.9)
Body height	26.7	29.8	22.0 (19.8–24.2)	25.2 (22.6–27.7)	27.7 (3.0)	30.1 (2.6)
Ramus height	61.0	69.6	57.2 (54.6–59.9)	61.0 (57.8–64.1)	58.5 (4.2)	65.2 (4.7)
Gonial angle	128.2	121.0	118.2 (114–122.3)	116.0 (112–121)	124.8 (8.4)	123 (7.2)
Intergonial distance	86.2	92.9	81.8 (78.4–85.1)	90.7 (87.3–94.1)	91.9 (5.8)	99.6 (6.0)
Pogonion–interdental distance	22.2	21.4	25.0 (23.4–26.6)	27.3 (25.0–29.5)	29.9 (3.7)	32.9 (4.7)

Shown are mandible body length, body height, ramus height, gonial angle, intergonial distance and pogonion–interdental distance. Angles are given in degrees and length measurements in millimetres

we assessed mandibles of partially edentulous patients selected for total joint replacement surgery of the TMJ, and the anatomy and SSMs of these patients are likely to be markedly different to those in healthy, dentate individuals. In the present study, mandibles were included from patients with Category 5 end-stage disease of the TMJ. This classification refers to a spectrum of disorders which

include osteoarthritis, rheumatoid arthritis and idiopathic condylar resorption and is primarily confined to the head of the condyle which may lose mass and take on an irregular surface as a result of the disease progression. The rest of the mandibular bony anatomy remains unaffected by the Category 5 joint disease. This study provides data that

may be useful in surgical planning and development of prosthetic TMJs, particularly in partially dentate patients.

Secondly, the duration of edentulism, which is known to influence the degree of alveolar atrophy and thus bone morphology (Aragao et al. 2014; Chrcanovic et al. 2011), was unknown in the patient data. In general, the presence of teeth adds to the vertical dimension to the body of the mandible in the way of alveolar bone so that the surrounding soft tissues, including the lips and cheeks, are well supported. When teeth have been missing for a long period of time, the alveolar bone undergoes resorption due to the lack of load transmission through the supporting teeth. As a result, bone mass and volume of a partially edentulous mandible can be significantly less than that of a dentate mandible. Edentulism may produce a more prominent mandible (i.e. Angle's Class 3) with sunken appearance of the surrounding soft tissues that lack the support of teeth. In end-stage conditions, this can result in the basal bone being the primary supporting framework for anchoring the tongue, floor of mouth and airway muscles.

Thirdly, the SSMs were trained on a small sample of partially edentulous subjects with 1–4 teeth absent (excluding the third molars) of mainly Caucasian descent; however, ethnicity is known to have a significant influence on edentulism prevalence (Kailembo et al. 2017; Wu et al. 2012) and may have been a confounding factor in the present study that increased dispersion of the geometric data. Fourthly, the degree of partial edentulism in each group was non-homogeneous and may have contributed to errors in model prediction between sexes. Finally, PCA-based statistical shape modelling approaches capture global shape variations but are not capable of characterising local and nonlinear shape variations which may have been present in the study groups.

In conclusion, the present study employed principal component analysis-based statistical shape modelling to characterise morphological variations across training sets of female and male partially edentulous mandibles. Dimorphic traits between sexes were confirmed, and seven morphometric measurements were ascertained as the most optimal subset of shape predictors for accurate prediction of 3D female and male mandible geometry, respectively. This study describes for the first time the use of SSMs in evaluation of inter-subject variability and morphology of partially edentulous mandibles. The modelling techniques may be useful in diagnosis and treatment of TMJ disorders, implant design and testing, pre-operative planning for reconstruction and implantation, and development of intraoperative surgical guides.

## Compliance with ethical standards

**Conflict of interest** The authors declare that they have no conflict of interest.

## References

- Ackland DC, Robinson D, Redhead M, Lee PV, Moskaljuk A, Dimitroulis G (2017) A personalized 3D-printed prosthetic joint replacement for the human temporomandibular joint: from implant design to implantation. *J Mech Behav Biomed Mater* 69:404–411. <https://doi.org/10.1016/j.jmbbm.2017.01.048>
- Aragao JA, Souto ML, Mateus CR, Menezes Ldos S, Reis FP (2014) Edentulousness in relation to remodeling of the gonial angles and incisures in dentate and edentate mandibles: morphometric study using the ImageJ software. *Surg Radiol Anat* 36:889–894. <https://doi.org/10.1007/s00276-014-1335-1>
- Bah MT et al (2015) Exploring inter-subject anatomic variability using a population of patient-specific femurs and a statistical shape and intensity model. *Med Eng Phys* 37:995–1007. <https://doi.org/10.1016/j.medengphy.2015.08.004>
- Balci Y, Yavuz MF, Cagdir S (2005) Predictive accuracy of sexing the mandible by ramus flexure. *Homo* 55:229–237
- Bayome M, Park JH, Kook YA (2013) New three-dimensional cephalometric analyses among adults with a skeletal Class I pattern and normal occlusion. *Korean J Orthod* 43:62–73. <https://doi.org/10.4041/kjod.2013.43.2.62>
- Bousleiman H, Iizuka T, Nolte LP, Reyes M (2013) Population-based design of mandibular fixation plates with bone quality and morphology considerations. *Ann Biomed Eng* 41:377–384. <https://doi.org/10.1007/s10439-012-0671-8>
- Bräuer G (1988) Osteometrie. In: Knussmann R (ed) *Anthropologie Handbuch der Vergleichenden Biologie des Menschen Band 1 Wesen und Methoden der Anthropologie*. Gustav Fischer, Stuttgart
- Brennan RM, Genco RJ, Hovey KM, Trevisan M, Wactawski-Wende J (2007) Clinical attachment loss, systemic bone density, and subgingival calculus in postmenopausal women. *J Periodontol* 78:2104–2111. <https://doi.org/10.1902/jop.2007.070155>
- Chan EF, Farnsworth CL, Kozioł JA, Hosalkar HS, Sah RL (2013) Statistical shape modeling of proximal femoral shape deformities in Legg–Calvé–Perthes disease and slipped capital femoral epiphysis. *Osteoarthr Cartil* 21:443–449. <https://doi.org/10.1016/j.joca.2012.12.007>
- Chrcanovic BR, Abreu MHNG, Custódio ALN (2011) Morphological variation in dentate and edentulous human mandibles. *Surg Radiol Anat* 33:203–213. <https://doi.org/10.1007/s00276-010-0731-4>
- Cocos A, Halazonetis DJ (2017) Craniofacial shape differs in patients with tooth agenesis: geometric morphometric analysis. *Eur J Orthod* 39:345–351. <https://doi.org/10.1093/ejo/cjw049>
- Dye B, Thornton-Evans G, Li X, Iafolla T (2015) Dental caries and tooth loss in adults in the United States, 2011–2012. *NCHS data brief*: 197
- Eke PI et al (2015) Update on prevalence of periodontitis in adults in the United States: NHANES 2009 to 2012. *J Periodontol* 86:611–622. <https://doi.org/10.1902/jop.2015.140520>
- Franklin D, O'Higgins P, Oxnard CE, Dadour I (2007) Sexual dimorphism and population variation in the adult mandible: forensic applications of geometric morphometrics. *Forensic Sci Med Pathol* 3:15–22. <https://doi.org/10.1385/fsm:3:1:15>
- Ghosh S, Vengal M, Pai KM (2009) Remodeling of the human mandible in the gonial angle region: a panoramic, radiographic, cross-sectional study. *Oral Radiol* 25:2–5. <https://doi.org/10.1007/s11282-009-0002-4>
- Guler AU, Sumer M, Sumer P, Bicer I (2005) The evaluation of vertical heights of maxillary and mandibular bones and the location of anatomic landmarks in panoramic radiographs of edentulous patients for implant dentistry. *J Oral Rehabil* 32:741–746. <https://doi.org/10.1111/j.1365-2842.2005.01499.x>

- Huomonen S et al (2010) Influence of edentulousness on gonial angle, ramus and condylar height. *J Oral Rehabil* 37:34–38. <https://doi.org/10.1111/j.1365-2842.2009.02022.x>
- Hwang E, Lin C, Jiao B, Chung N-E, Han S-H, Kim J, Lee UY (2015) Discriminant function analysis for sex determination using landmark coordinate data from three-dimensional mandible models. *Aust J Forensic Sci* 47:332–344. <https://doi.org/10.1080/00450618.2014.960449>
- Jolliffe IT (2002) Principal component analysis. Springer, Berlin
- Kailembo A, Preet R, Stewart Williams J (2017) Common risk factors and edentulism in adults, aged 50 years and over, in China, Ghana, India and South Africa: results from the WHO Study on global AGEing and adult health (SAGE). *BMC Oral Health* 17:29. <https://doi.org/10.1186/s12903-016-0256-2>
- Kemkes-Grotenthaler A, Lobig F, Stock F (2002) Mandibular ramus flexure and gonial eversion as morphologic indicators of sex. *Homo* 53:97–111
- Kim S-G et al (2012) Development of 3D statistical mandible models for cephalometric measurements. *Imaging Sci Dent* 42:175–182
- Koc D, Dogan A, Bek B (2010) Bite force and influential factors on bite force measurements: a literature review. *Eur J Dent* 4:223–232
- Lima FJC, Oliveira Neto OB, Barbosa FT, Sousa-Rodrigues CF (2016) Location, shape and anatomic relations of the mandibular foramen and the mandibular lingula: a contribution to surgical procedures in the ramus of the mandible. *Oral Maxillofac Surg* 20:177–182. <https://doi.org/10.1007/s10006-016-0547-4>
- Lin H, Zhu P, Lin Y, Wan S, Shu X, Xu Y, Zheng Y (2013) Mandibular asymmetry: a three-dimensional quantification of bilateral condyles. *Head Face Med* 9:42. <https://doi.org/10.1186/1746-160X-9-42>
- Lin C, Jiao B, Liu S, Guan F, Chung NE, Han SH, Lee UY (2014) Sex determination from the mandibular ramus flexure of Koreans by discrimination function analysis using three-dimensional mandible models. *Forensic Sci Int* 236:191.e191–191.e196. <https://doi.org/10.1016/j.forsciint.2013.12.015>
- Loth SR, Henneberg M (1996) Mandibular ramus flexure: a new morphologic indicator of sexual dimorphism in the human skeleton. *Am J Phys Anthropol* 99:473–485. [https://doi.org/10.1002/\(sici\)1096-8644\(199603\)99::<473:aid-ajpa>3.0.co;2-x](https://doi.org/10.1002/(sici)1096-8644(199603)99::<473:aid-ajpa>3.0.co;2-x)
- McGarry TJ, Nimmo A, Skiba JF, Ahlstrom RH, Smith CR, Koumjian JH, Arbree NS (2002) Classification system for partial edentulism. *J Prosthodont* 11:181–193
- Metzger MC, Vogel M, Hohlweg-Majert B, Mast H, Fan X, Rüdell A, Schlager S (2011) Anatomical shape analysis of the mandible in Caucasian and Chinese for the production of preformed mandible reconstruction plates. *J Craniomax Surg* 39:393–400. <https://doi.org/10.1016/j.jcms.2010.10.005>
- Mohammad AR, Hooper DA, Vermilyea SG, Mariotti A, Preshaw PM (2003) An investigation of the relationship between systemic bone density and clinical periodontal status in post-menopausal Asian-American women. *Int Dent J* 53:121–125. <https://doi.org/10.1111/j.1875-595X.2003.tb00735.x>
- Nicholson E, Harvati K (2006) Quantitative analysis of human mandibular shape using three-dimensional geometric morphometrics. *Am J Phys Anthropol* 131:368–383. <https://doi.org/10.1002/ajpa.20425>
- Oettle AC, Becker PJ, de Villiers E, Steyn M (2009a) The influence of age, sex, population group, and dentition on the mandibular angle as measured on a South African sample. *Am J Phys Anthropol* 139:505–511. <https://doi.org/10.1002/ajpa.21009>
- Oettle AC, Pretorius E, Steyn M (2009b) Geometric morphometric analysis of the use of mandibular gonial eversion in sex determination. *Homo* 60:29–43. <https://doi.org/10.1016/j.jchb.2007.01.003>
- Ozturk CN, Ozturk C, Bozkurt M, Uygur HS, Papay FA, Zins JE (2013) Dentition, bone loss, and the aging of the mandible. *Aesthetic Surg J* 33:967–974. <https://doi.org/10.1177/1090820X13503473>
- Parr NM, Passalacqua NV, Skorpinski K (2017) Investigations into age-related changes in the human mandible. *J Forensic Sci*. <https://doi.org/10.1111/1556-4029.13475>
- Peltzer K et al (2014) Prevalence of loss of all teeth (edentulism) and associated factors in older adults in China, Ghana, India, Mexico, Russia and South Africa. *Int J Environ Res Public Health* 11:11308–11324. <https://doi.org/10.3390/ijerph111111308>
- Polychronis G, Christou P, Mavragani M, Halazonetis DJ (2013) Geometric morphometric 3D shape analysis and covariation of human mandibular and maxillary first molars. *Am J Phys Anthropol* 152:186–196. <https://doi.org/10.1002/ajpa.22340>
- Raith S, Varga V, Steiner T, Hölzle F, Fischer H (2016) Computational geometry assessment for morphometric analysis of the mandible. *Comput Methods Biomech Biomed Eng* 20:27–34. <https://doi.org/10.1080/10255842.2016.1196196>
- Raith S, Wolff S, Steiner T, Modabber A, Weber M, Hölzle F, Fischer H (2017) Planning of mandibular reconstructions based on statistical shape models. *Int J Comput Assist Radiol Surg* 12:99–112. <https://doi.org/10.1007/s11548-016-1451-y>
- Russell S, Gordon S, Lukacs J, Kaste L (2013) Sex/gender differences in tooth loss and edentulism: historical perspectives, biological factors, and sociologic reasons. *Dent Clin*. <https://doi.org/10.1016/j.cden.2013.02.006>
- Schneider MT, Zhang J, Crisco JJ, Weiss AP, Ladd AL, Nielsen P, Besier T (2015) Men and women have similarly shaped carpometacarpal joint bones. *J Biomech* 48:3420–3426. <https://doi.org/10.1016/j.jbiomech.2015.05.031>
- Sella-Tunis T, Pokhojaev A, Sarig R, O'Higgins P, May H (2018) Human mandibular shape is associated with masticatory muscle force. *Sci Rep* 8:6042. <https://doi.org/10.1038/s41598-018-24293-3>
- Smoger LM, Shelburne KB, Cyr AJ, Rullkoetter PJ, Laz PJ (2017) Statistical shape modeling predicts patellar bone geometry to enable stereo-radiographic kinematic tracking. *J Biomech* 58:187–194. <https://doi.org/10.1016/j.jbiomech.2017.05.009>
- Tibshirani R (1996) Regression shrinkage and selection via the lasso. *J R Stat Soc Ser B (Methodol)* 58:267–288
- Watanabe H, Mohammad Abdul M, Kurabayashi T, Aoki H (2010) Mandible size and morphology determined with CT on a premise of dental implant operation. *Surg Radiol Anat* 32:343–349. <https://doi.org/10.1007/s00276-009-0570-3>
- Woods C, Fernee C, Browne M, Zakrzewski S, Dickinson A (2017) The potential of statistical shape modelling for geometric morphometric analysis of human teeth in archaeological research. *PLoS ONE* 12:e0186754. <https://doi.org/10.1371/journal.pone.0186754>
- Wu B, Liang J, Plassman BL, Remle RC, Luo X (2012) Edentulism trends among middle-aged and older adults in the united states: comparison of five racial/ethnic groups. *Commun Dent Oral Epidemiol* 40:145–153. <https://doi.org/10.1111/j.1600-0528.2011.00640.x>
- Zachow S, Lamecker H, Elsholtz B, Stiller M (2005) Reconstruction of mandibular dysplasia using a statistical 3D shape model. *Int Congr Ser* 1281:1238–1243. <https://doi.org/10.1016/j.ics.2005.03.339>
- Zhang J, Malcolm D, Hislop-Jambrich J, Thomas CDL, Nielsen PMF (2014) An anatomical region-based statistical shape model of the human femur. *Comput Methods Biomech Biomed Eng Imaging Vis* 2:176–185. <https://doi.org/10.1080/21681163.2013.878668>
- Zhang J, Hislop-Jambrich J, Besier TF (2016) Predictive statistical models of baseline variations in 3-D femoral cortex morphology. *Med Eng Phys* 38:450–457. <https://doi.org/10.1016/j.medengphy.2016.02.003>
- Zhang J, Ackland DC, Fernandez J (2018) Point-cloud registration using adaptive radial basis functions. *Comput Methods Biomech Biomed Eng* 21:498–502

**Publisher's Note** Springer Nature remains neutral with regard to jurisdictional claims in published maps and institutional affiliations.